

Charge and Spin Dynamics and Destabilization of Shallow Nitrogen–Vacancy Centers under UV and Blue Excitation

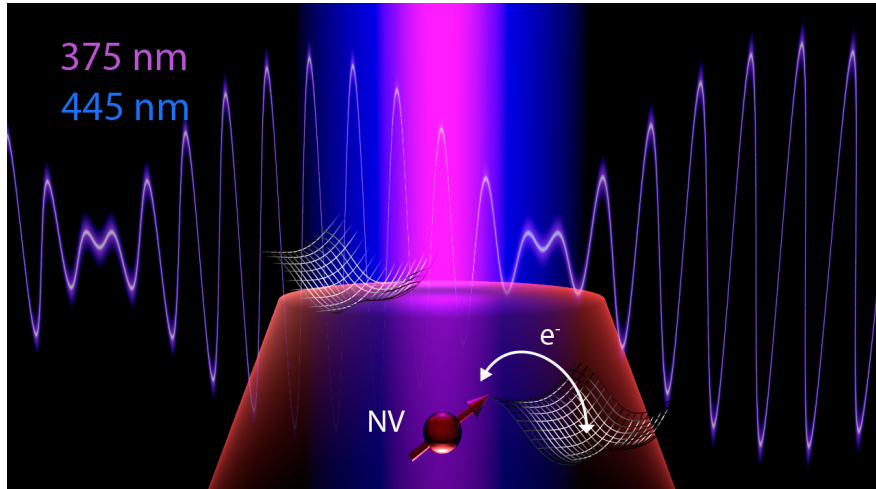
Laura A. Völker,[†] Konstantin Herb,[†] Darin A. Merchant,[†] Lorenzo Bechelli,[†]

Christian L. Degen,^{*,†,‡} and John M. Abendroth^{*,†}

[†]*Department of Physics, ETH Zürich, Otto-Stern-Weg 1, 8093 Zürich, Switzerland*

[‡]*Quantum Center, ETH Zürich, 8093 Zürich, Switzerland*

E-mail: degen@phys.ethz.ch; jabendroth@phys.ethz.ch



Abstract

Shallow nitrogen–vacancy (NV) centers in diamond offer unique opportunities for studying photochemical reactions at the single-molecule level, such as the photogeneration of radical pairs in proximal molecules. A prerequisite for such experimental schemes is the detailed understanding of the charge and spin dynamics of NV centers exposed to the short-wavelength light required for photoexciting chemical species. Here, we measure and analyze the charge and spin dynamics of shallow NV centers under 445 nm (blue) and 375 nm (UV) illumination. With blue excitation, we observe a power-dependent charge-state preparation accompanied by modest preservation of spin initialization fidelity. Under UV excitation, we find a power-independent charge-state preparation and no spin polarization. We further observe an irreversible aging of NV centers under prolonged exposure to UV, and to a lesser extent, blue laser excitation, which we attribute to formation of new electronic trap states. This aging manifests itself in a reduced charge stability and spin contrast, and is detrimental to the NV sensing performance. We evaluate the prospects and limitations of NV centers for probing photogenerated radical pairs based on experimentally measured sensitivities following blue and UV excitation, and outline the design rules for possible sensing schemes.

Keywords

nitrogen–vacancy (NV) center, quantum sensing, photoionization, optically detected magnetic resonance (ODMR), radical pairs

Photoexcitation by blue and UV light plays a pivotal role in biology, where illumination initiates chemical transformations, often *via* formation of short-lived radicals and radical pairs (RPs).¹⁻⁶ Further, photogenerated RPs in synthetic chemical architectures excited by these wavelengths are of interest as molecular qubits for quantum information processing.⁷⁻¹⁰ To address these systems *via* magnetic resonance spectroscopy in the single- to few-molecule regime, quantum sensing with near-surface nitrogen–vacancy (NV) centers in diamond has been proposed to track charge separation and recombination, spin dynamics, and spin polarization in photogenerated RPs.¹¹⁻¹⁴ The NV exhibits high magnetic field sensitivity, nanoscale localization, and room-temperature operability, offering complementary information to conventional EPR and NMR spectroscopies.¹⁵⁻¹⁹ Thus, magnetic field sensing with shallow NVs could provide insight into the complex spin dynamics and photochemical cascades involved in RP generation.

Experimental realization of NV-RP sensing requires a detailed understanding of charge ionization rates, spin dynamics, and photostability of shallow defects under blue or UV illumination.²⁰⁻²² Despite a significant body of work on NV center photoionization over a wide range of excitation wavelengths,²³⁻²⁸ effects of blue and UV irradiation are little characterized by comparison. Previous works that explored the influence of irradiation in the near-UV and blue regions utilized all-optical methods to track interconversion between the desired negatively charged NV^- and undesired neutral NV^0 states.^{26,29-34} Still, detailed effects on NV spin dynamics, such as the spin initialization fidelity, remain to be explored in detail. Importantly, exposure to short wavelengths may also accelerate deterioration of shallow NV properties, and necessitates further analysis. Such effects are evidenced by, *e.g.*, blinking, loss in optically detected magnetic resonance (ODMR) contrast, and accelerated ionization rates due to changes to the NV’s electronic environment.³⁵⁻³⁹

In this work, we expand on previous studies of blue and UV photophysics of diamond defects^{26,29-34} by investigating the effects of 445 nm and 375 nm excitation on the charge and spin dynamics of individual, shallow (*ca.* 10-nm-deep) NV centers. Under 445 nm

laser excitation, we observe power-dependent charge-state initialization, rationalized by one-photon ionization and two-photon recombination dynamics. Decent spin-state initialization fidelities are maintained at ca. 50% of the original ODMR contrast under steady-state conditions. Under UV excitation, we observe power-independent charge-state initialization and complete absence of optical spin polarization. We further find that prolonged exposure to either wavelength permanently alters the NV ionization dynamics. These effects are attributed to the formation of modified electronic environments, likely *via* generation of additional electron traps. Finally, we outline the prospects of shallow defects for NV-RP sensing under realistic experimental conditions.

Figure 1a,b illustrates the photoionization dynamics between NV^- , which exhibits a zero phonon line (ZPL) at 637 nm, and NV^0 with a ZPL at 575 nm.²³ Interconversion between the charge states reduces the ODMR contrast by decreasing spin-state initialization fidelity of NV^- and increasing fluorescence background due to a high steady-state NV^0 population.³⁸ The essential dynamics of the system are captured by a three-level model (**Figure 1a**, and SI) that comprises two levels (M_0 and M_1) for NV^- in the $m_S = 0$ and $m_S = \pm 1$ states, respectively, and one level (Z) for NV^0 . Charge and spin dynamics are described by spin-dependent ionization rates $k_{i,0}$ and $k_{i,1}$, spin-state polarization with rate k_s , and charge recombination at rate k_r . The three-level model forms the basis for distinguishing four dynamic regimes in the UVA-visible spectrum, categorized by one- *versus* two-photon ionization or recombination of NV charge states. At wavelengths between the ZPL of NV^0 and NV^- (region D), photons primarily excite NV^- but not NV^0 . This selective excitation of NV^- enables charge-state-sensitive protocols.^{40,41} However, high laser powers trap the population in NV^0 due to two-photon ionization, and re-ionization of NV^- requires irradiation with shorter wavelengths.²⁹ Therefore, sensing with NVs commonly utilizes wavelengths ~ 532 nm (region C, 476 nm–575 nm), where both charge states are excited and interconverted *via* two-photon ionization and recombination allowing for NV^- populations of *ca.* 70%.^{24,26} In addition, optical spin polarization (initialization) can be achieved with high

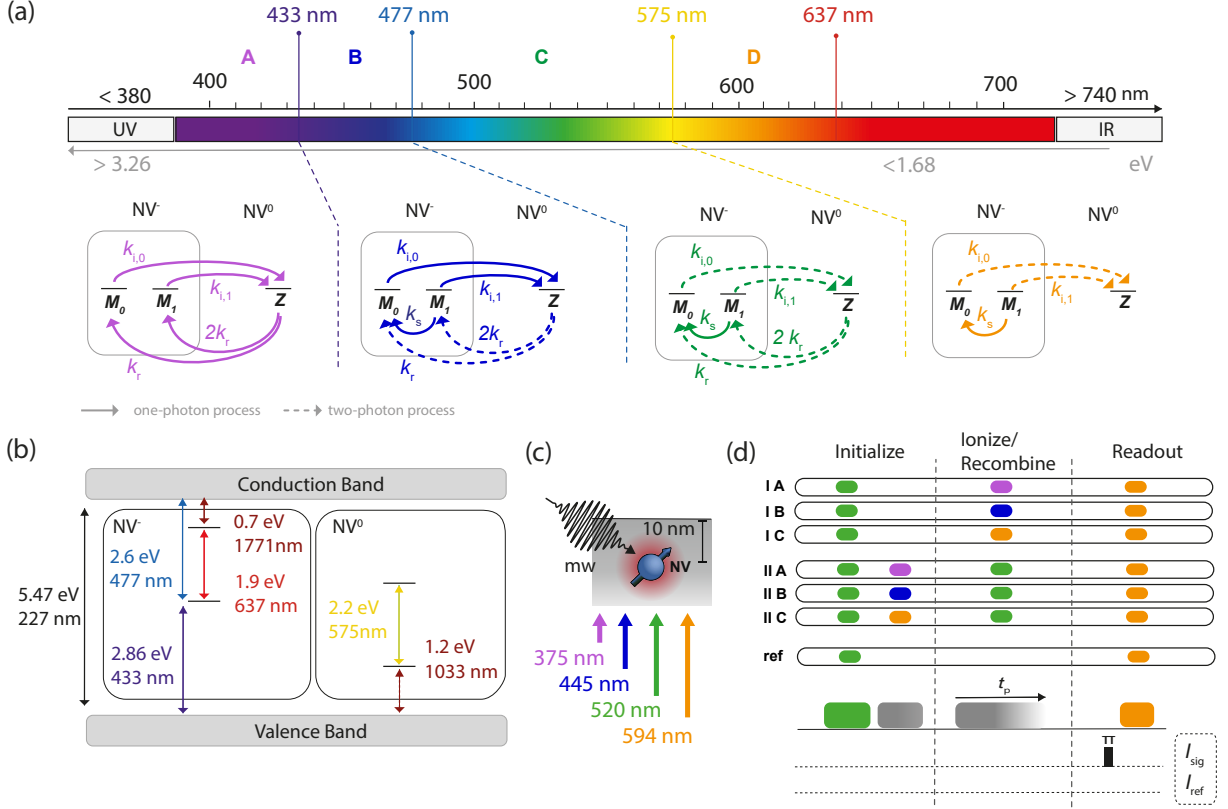


Figure 1: Optically-driven charge-state dynamics of the NV center and experimental protocol. (a) *Top:* The relevant wavelength ranges can be divided into four regions, A-D, depending on the ionization and recombination pathways which are accessible at a given wavelength. *Bottom:* Schematic depiction of a simplified three-level system, modeling NV^- with two levels (M_0 and M_1) for spin states $m_S = 0$ and $m_S = \pm 1$, respectively and NV^0 as a single level (Z). Spin-dependent ionization rates are denoted as $k_{i,0}$ and $k_{i,1}$, k_s is the rate of spin-state polarization, and k_r is the recombination rate from NV^0 to NV^- . Solid lines represent one-photon excitations, dashed lines indicate two-photon excitations. (b) Energy level diagram of the electronic ground and excited states of NV^- and NV^0 within the band gap of the diamond host material. (c) Schematic of the experimental set-up: A diamond membrane hosting single, shallow NV centers is exposed to different laser colors in a confocal microscope with integrated microwave infrastructure. (d) Experimental protocol, *i.e.* pulse sequences utilized to study charge and spin state manipulation of shallow NV centers.

fidelity, especially at low laser powers.⁴² At wavelengths shorter than 477 nm, but longer than 433 nm (region B), optical spin initialization competes with the onset of one-photon ionization of NV^- *via* loss of an electron to the conduction band,^{26,28} while recombination of NV^0 to NV^- remains a two-photon process.¹ Only at wavelengths below 433 nm (region A) are one-photon pathways accessible for both ionization and recombination. Although the energy levels that dictate these thresholds are well-established,²⁸ experimental studies have categorized wavelengths below *ca.* 450 nm as a uniform regime with charge-state dynamics that are dominated by one-photon ionization of NV^- from the ground state.^{30,31,34} In the following, we demonstrate that regions A and B feature distinct photodynamics, especially at higher laser powers. Further, we show that loss of spin-initialization fidelity at these wavelengths is due to a combination of reduced photoluminescence excitation (PLE)²⁵ and one-photon ionization processes.

Our measurement scheme and available laser wavelengths are depicted in **Figure 1c,d**. Experiments are performed on a commercially available (QZabre Ltd) (001)-terminated single-crystalline CVD-grown diamond membrane implanted with $^{15}\text{N}^+$ ions at 7 keV energy and featuring nanofabricated pillar waveguide arrays to enhance optical collection efficiency and register single NVs.⁴⁴ The membrane sample is annealed in O_2 at 460 °C before characterization to remove graphitic carbon and terminate the surface with oxygen.^{17,37} Experimental protocols are schematically outlined in **Figure 1d**. First, we probe photoionization dynamics and spin state perturbation under 375 nm or 445 nm excitation with comparison to orange (594 nm) illumination as a common reference (IA–IC, **Figure 1d**). In each protocol, charge and spin state of NVs are first initialized using a green (520 nm) laser; then a perturbing 375 nm, 445 nm, or 594 nm laser pulse of varying length t_p and power P is applied. Second, we analyze re-initialization of the NV from the perturbed states, *i.e.*, the recombination

¹Note that other experimental and theoretical studies have determined one-photon ionization thresholds to be 2.64 eV (470 nm),⁴³ 2.7 eV (459 nm)³¹ and 2.74 eV (452 nm)³¹ instead which are in good agreement with the value of 2.6 eV (477 nm) of Aslam *et al.*²⁶ that we utilize here. The threshold for one-photon recombination has not yet been experimentally measured, but was calculated here by subtracting the energy difference between the ground state of NV^- and the conduction band from the bandgap of diamond.

dynamics (IIA–IIC, **Figure 1d**). Here, the NV is first prepared in its equilibrium charge and spin state under 375 nm, 445 nm, or 594 nm illumination before being re-initialized with a green laser pulse of length t_p . In all experiments, the resulting state of the NV is read out in a pulsed ODMR experiment. To manipulate the spin state, we apply resonant microwave pulses supplied by a coplanar waveguide and apply a 10 mT magnetic bias field oriented along the NV axis to lift the $m_s = \pm 1$ degeneracy. For readout, we use a low-power orange pulse enabling simultaneous detection of the NV spin and charge states.^{40,41} All relevant laser pulse durations, powers and delay times for data presented in the main text are detailed in the SI.

Our two experimental measurables are the population of the NV^- charge state ρ and the ODMR contrast c describing the degree of spin polarization in NV^- . In the context of our three-level model, we define ρ and c by

$$\rho = \frac{M_0 + M_1}{M_0 + M_1 + Z} \quad (1a)$$

$$c = \frac{M_0 - M_1}{M_0}, \quad (1b)$$

with level populations M_0 , M_1 and Z . Under orange laser excitation, only populations M_0 and M_1 contribute to the fluorescence signal. Thus, our experimental observables are directly proportional to M_0 and M_1 . Following a short derivation (see SI), we approximate ρ and c for each laser pulse duration by

$$\rho(t_p) \approx \frac{\frac{1}{3}I_{\text{ref}}(t_p) + \frac{2}{3}I_{\text{sig}}(t_p)}{\frac{1}{3}I_{\text{ref}}^0(t_p) + \frac{2}{3}I_{\text{sig}}^0(t_p)} \quad (2a)$$

$$c(t_p) \approx \frac{I_{\text{ref}}(t_p) - I_{\text{sig}}(t_p)}{I_{\text{ref}}(t_p)} \quad (2b)$$

where $I_{\text{sig}}(t_p)$ and $I_{\text{ref}}(t_p)$ are the photoluminescence intensities in signal and reference traces

of the ODMR experiment. Since the absolute value of ρ cannot be determined experimentally, we calculate ρ relative to the charge state under green laser illumination by normalizing with respect to ODMR signals I_{ref}^0 and I_{sig}^0 obtained in a separate reference measurement (ref, **Figure 1d**). From $\rho(t_p)$ we extract ionization rates k_i^λ ($\lambda=375$ nm, 445 nm, 594 nm) for protocols IA–IC and recombination rates k_r^{520} for protocols IIA–IIC. The equilibrium charge and spin states ρ^λ and c^λ are obtained at long t_p , *i.e.*, ($t_p \rightarrow \infty$) under a given illumination wavelength λ .

We begin our study by investigating the charge and spin dynamics in wavelength regime B. **Figure 2a,b** shows data for a representative NV subjected to 445 nm excitation between 0.1 and 1 mW (protocol IB). At low powers ($P^{445} \sim 0.1$ mW) significant ionization to $\rho^{445} \leq 20\%$ occurs, aligning with previous work.^{26,30,31} Yet, ρ^{445} increases up to $\geq 75\%$ if P^{445} is raised to ~ 1 mW. This observation is in agreement with our preceding theoretical considerations for regime B. Here, the energy of a single photon is sufficient for ionization, while charge recombination requires two photons. The resulting linear *versus* quadratic power dependencies of ionization and recombination rates make ρ^{445} power-dependent. The variation of the equilibrium charge state with P^{445} is a characteristic of wavelength regime B, which to the best of our knowledge has not yet been experimentally explored.

We also find evidence for a minor contribution of two-photon ionization with 445 nm excitation. At high laser powers, $\rho(t_p)$ evolves in a bi-exponential manner featuring fast initial decay and slower recovery toward the steady-state value. Our three-level model predicts a bi-exponential evolution of $\rho(t_p)$ only if ionization is spin-dependent, *i.e.* $k_{i,0} \neq k_{i,1}$. Notably, this spin-dependent two-photon ionization is possible due to non-zero PLE of NV^- at this wavelength.²⁵ The reduced, yet finite PLE of NV^- under blue light illumination manifests itself in a surprisingly high steady-state ODMR contrast of approximately 50% of the original value, independent of P^{445} . A promising consequence of this result is that conventional ODMR experiments are compatible with continuous-wave illumination at 445 nm.

Figure 2c,d presents an analogous investigation for wavelength regime A, using 375 nm

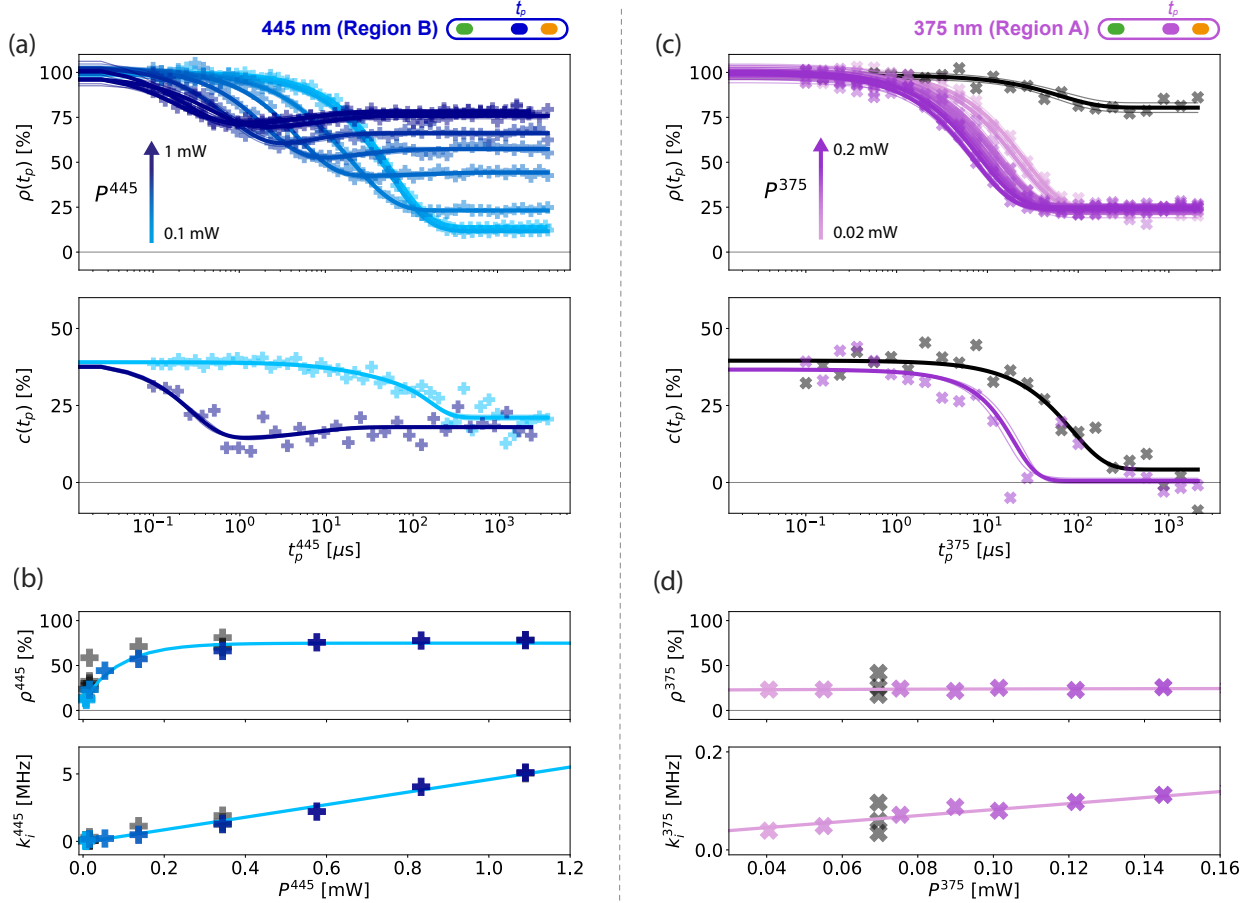


Figure 2: Charge and spin dynamics under 445 nm illumination (*left*) and 375 nm illumination (*right*) for representative NVs. (a,c) Evolution of NV⁻ population ρ (*Top*) and ODMR contrast c (*Bottom*) under 445 nm (375 nm) laser illumination at different laser powers, P^{445} (P^{375}), encoded in marker color. Fitting was performed on the raw experimental data, $I_{\text{ref}}(t_p)$, $I_{\text{sig}}(t_p)$, from which fits for ρ and c were calculated (Equations 2a, 2b). (b,d) Power dependence of charge and spin dynamics under 445 nm (375 nm) illumination, characterized *via* NV⁻ population ρ^{445} (ρ^{375}) and ionization rate k_i^{445} (k_i^{375}). Initial measurements that were performed before the NV had sufficiently stabilized in an aged state are shown in grey. An especially pronounced change is evident for UV charge dynamics, where pristine NV centers ionize to a much lesser extent despite complete loss of ODMR contrast.

laser excitation (protocol IA). These data are recorded using a second NV. In contrast to our earlier findings for regime B, a mono-exponential decay of $\rho(t_p)$ at all laser powers to a power-independent steady state value of $\sim 20\%$ is evident for regime A. Again, these observations are well-explained by our three-state model. In regime A, recombination can now occur *via* one-photon processes, making ρ^{375} independent of laser power. Ionization is also spin-independent ($k_{i,0} = k_{i,1}$) since it occurs solely *via* one-photon processes. Vanishing c from the remaining NV^- population at all powers is indicative of a complete loss of spin polarization ($k_s = 0$). Since ionization events do not necessarily preserve spin state, rapid one-photon charge-state interconversion driven by 375 nm excitation destroys spin-state fidelity.

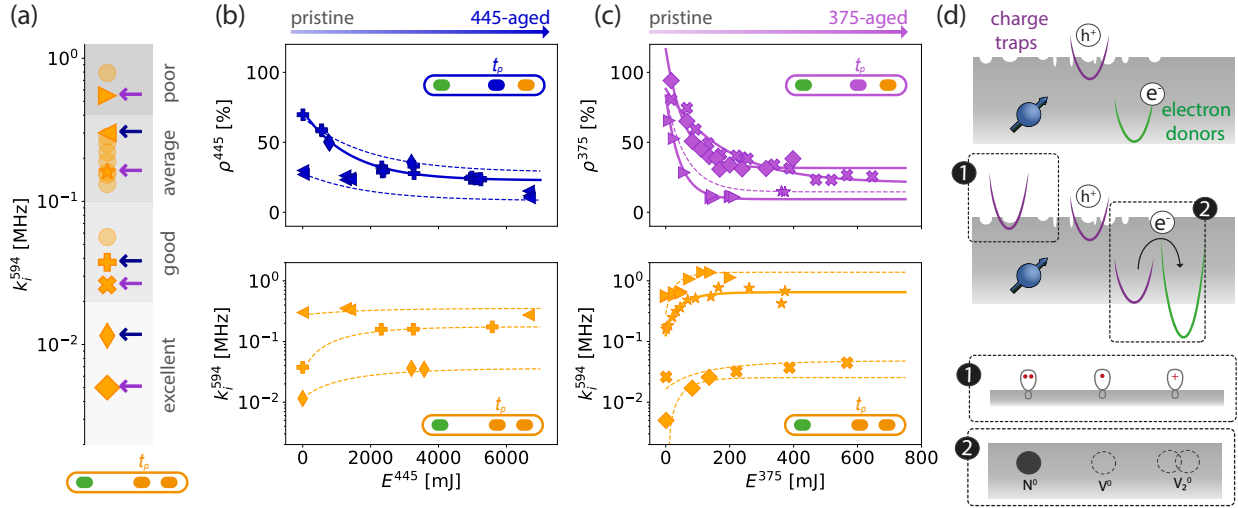


Figure 3: Aging of NV charge environments under prolonged exposure to 375 nm or 445 nm laser illumination. (a) Ionization rates k_i^{594} under orange laser illumination are utilized as classifiers for the local charge-environment of the NV (ranging from poor to excellent). Blue (violet) arrows indicate which NVs were selected to probe the effects of 445 nm (375 nm) light exposure. (b, c) In-depth analysis of the charge environment evolution induced by blue (b) or UV (c) exposure. Steady state NV^- populations ρ^{445} (ρ^{375}) and ionization rates k_i^{594} evolve in an exponential manner as a function of exposure dose E^{445} (E^{375}). Solid lines indicate least-squares exponential fits of the experimental data. Dashed lines visualize the evolution in all cases where no direct fit could be performed. (d) *Top*: Additional formation of electron traps may occur via 1) modification of the diamond surface, 2) depletion of existing electron traps. *Bottom*: Modification of the diamond surface could include formation of reactive carbanions, carbon radicals or carbocations. Substitutional nitrogen atoms,⁴⁵ vacancies⁴⁶ and divacancies⁴⁷ are expected to be efficiently excited with UV-blue wavelengths.

Notably, we observed that the photophysical parameters changed during prolonged UV or blue laser exposure. For data presented in **Figure 2** and SI, defects had been exposed to sufficient doses of blue or UV laser light to reach stable photophysical behavior. These data deviate from results obtained on pristine NVs at the beginning of each measurement series. Prior to prolonged UV or blue exposure, NVs consistently exhibit higher ρ and lower k_i than after illumination (shown in black in **Figure 2**). Rapid deterioration is especially pronounced for UV excitation, where initial characterization of NVs reveals $\rho \geq 75\%$ following UV laser pulses (**Figure 2c**), similar to earlier findings of comparably minor ionization under UV illumination.³⁰

To understand this apparent "aging" of NVs and their electronic environment, we measure the ionization rates k_i^{594} under orange laser illumination (protocol IC) as a function of the total amount of energy E delivered by blue or UV laser excitation. This ionization rate is sensitive to the local charge environment of the emitter, which varies significantly for shallow NVs even with comparable depths.^{36,38,39} Our observed values of k_i^{594} span two orders of magnitude for the entire set of pristine NVs (**Figure 3a**). For analysis, we group NVs according to their orange ionization rates in categories ranging from excellent to poor (low to high k_i^{594}) and select defects from each group for full characterization. We measure exponential increases in k_i^{594} by up to one order-of-magnitude with increasing E (**Figure 3b,c**). Notably, $10\times$ greater E is required to reach the aged state under 445 nm irradiation compared to 375 nm irradiation. As expected for both wavelengths, the increase in k_i^{594} is accompanied by a decrease in the equilibrium NV⁻ fraction ρ^λ on the same energy scale.

The acceleration of the ionization dynamics is indicative of the formation of novel electron trap states under prolonged blue and UV exposure. Two mechanisms could explain this behavior: 1) the generation of persistent reactive species (*i.e.*, carbon radicals, carbanions, or carbocations) at the diamond surface²⁰ that can modify charge stability *via* band bending at the interface⁴⁸ or 2) a more rapid depletion of existing electron donors in favor of deeper electron traps that were previously inaccessible (**Figure 3d**). The former mecha-

nism is relevant in the context of photochemical surface functionalization techniques driven by UV and blue illumination.²⁰ Exploring whether the reduced NV stability persists even after the reactive species had undergone further reaction would provide insight into their contribution to NV aging. The latter mechanism is hypothesized based on efficient excitation of substitutional nitrogen donors (N^0),⁴⁵ vacancies (V^0)⁴⁶ and di-vacancies (V_2^0)⁴⁷ with short wavelengths of light, thereby redistributing holes and altering their accessibility. In combination, these mechanisms could contribute to destabilization including sudden drops of ODMR contrast, blinking, and even complete and irreversible loss of photoluminescence. Such effects are known to occur for shallow emitters,^{37,38} yet the chemical or physical nature of responsible trap states remains poorly understood. Further studies are required to establish connections between UV- or blue-light-induced aging and the deterioration of NV properties seen during conventional sensing with green laser excitation. If the same changes in the NVs charge environments are responsible for laser-induced aging, our insights could provide guidance for stabilization of shallow defects.

To further analyze the nature of newly formed trap states, we study the charge recombination dynamics under green illumination (protocols IIA–C). Initial characterization of defects (*i.e.*, before aging) reveals that recovery of the charge and spin states by green pulses is mono-exponential and exhibits rates $k_r^{520} \approx 1$ MHz, indifferent to preceding perturbation by 375 nm, 445 nm, or 594 nm pulses (SI Figure S4, S5, S6). After blue light-induced aging, these charge recombination dynamics remain unchanged as evidenced by mono-exponential recovery of ρ on multiple NVs following ionization with 445 nm pulses (**Figure 4a**). In contrast, UV-induced aging leads to modified charge recombination rates depending on the NV classification (excellent \rightarrow poor). Recovery from UV-induced ionization becomes bi-exponential and slower for poor and, to a lesser extent, average, NVs (**Figure 3b**). For these NVs, a steady-state $\rho(t_p)$ is only reached after ≈ 1 ms, corresponding to $k'_r \approx 1$ kHz. The bi-exponential dynamics suggest the existence of a second recombination channel, consistent with the formation of a previously inaccessible electron trap. Importantly, these

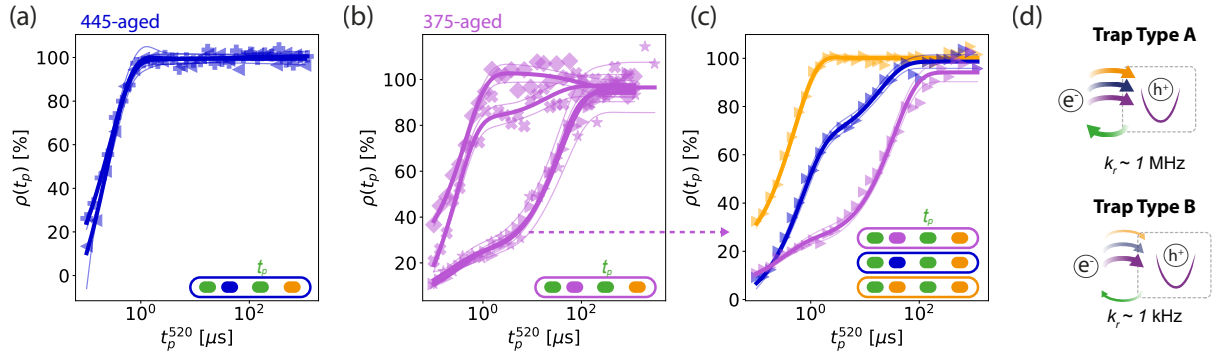


Figure 4: Re-initialization of the charge state using green illumination for aged NVs. (a) Recombination after 445 nm light induced ionization, measured on NVs that were aged with 445 nm illumination. (b) Recombination after 375 nm light induced ionization, measured on NVs that were aged with 375 nm illumination. To varying degree, the re-initialization now occurs at a ms timescale. (c): For an NV showing slow recombination after UV induced ionization, the recombination measurement is repeated but using blue or orange light for ionization. (d) We propose two distinct electron trap states with different recombination rates under green illumination. Trap type A is present on pristine and aged NV centers, accessible at orange, blue and UV wavelengths and allows for fast recombination under green illumination at a μs -timescale. Trap type B is only formed during UV-aging, only populated under UV or blue wavelengths and accounts for a slow recombination channel at a ms-timescale.

recombination rates depend on the wavelength of the preceding ionizing pulse. The fraction of the new, slowly recovering component is strongest for a 375 nm pulse, still present for a 445 nm pulse, and fully absent for ionization by 594 nm pulses (**Figure 4b**). Thus, population of the novel electron traps following UV aging requires higher photon energies compared to the electron trap states existing on pristine NVs (**Figure 4c**). Since recombination on blue-aged NVs following 445 nm pulses do not feature this bi-exponential recovery behavior, we conclude that the types of traps formed upon prolonged blue *versus* UV exposure are different.

We finally assess the potential of near-surface NVs for probing photo-induced effects in proximal molecules using 445 nm or 375 nm excitation.^{11–14} In the proposed experiment, molecules that support formation of photogenerated RPs, *e.g.*, synthetic electron donor–bridge–acceptor species³⁰ or biologically relevant blue-light sensitive cryptochromes,⁵ are functionalized on the diamond surface close to a near-surface NV (**Figure 5a**).^{17–20} After

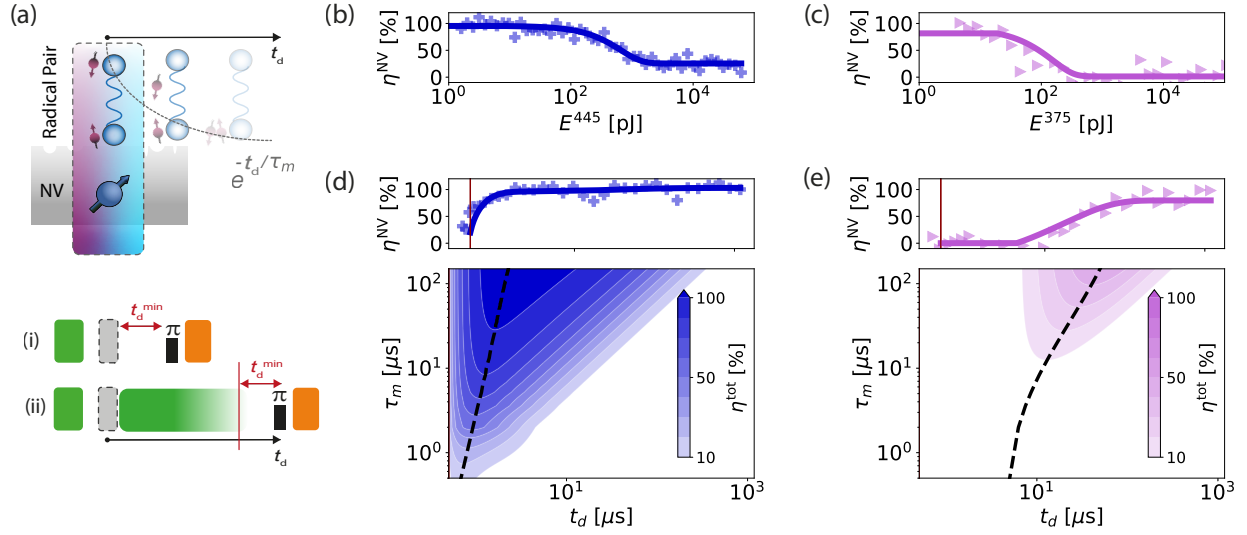


Figure 5: Consequences of blue and UV photo-induced spin and charge dynamics on sensing of photo-excitabile molecular analytes. (a) Schematic of the proposed experiment. The surface of a diamond sample containing shallow NVs is functionalized with molecules that support generation of radical pairs using UV or blue light at $t_d = 0$ following initialization of the NV with a green pulse. Population of the photo-generated radical pair species decays exponentially *via* charge recombination with lifetime τ_m . Sensing may be performed using two schemes *i* and *ii*; in the latter, the NV's charge and spin state are subsequently re-prepared using a second green laser pulse. In both, a microwave π pulse and orange laser readout complete the ODMR sensing sequence. (b,c) Experimentally measured evolution of NV sensitivity η^{NV} as a function of energy deposited by a blue (b) or UV (c) laser pulse on representative aged NVs. (d,e) *Top*: Experimentally measured recovery of sensitivity η^{NV} on the same NVs after a perturbing low-power 445 nm (16 μ W and 500 ns) (b) or 375 nm (34 μ W and 250 μ s) (c) laser pulse. *Bottom*: Total sensitivity η^{tot} calculated for radical pair lifetimes τ_m spanning 500 ns to 100 μ s for blue (d) and UV (e) laser pulses. Black dashed lines follow the maximum η^{tot} for each scheme.

initialization of the NV, photoexcitation with a blue or UV pulse generates RPs in the molecules with lifetime τ_m before charge recombination. To measure the effect of these transient noise sources on the NV’s ODMR contrast or frequency, a single microwave π -pulse at the NV $m_S = 0$ to $m_S = \pm 1$ transition frequency follows the blue or UV pulses after delay t_d with low-power orange readout pulse.

A general expression for sensitivity of the NV in this experiment is given by $\eta^{\text{NV}} \propto \sqrt{\rho c}$. **Figure 5b,c** shows experimentally measured evolution of η^{NV} as a function of the energy $E^\lambda = P^\lambda t_p$ delivered by a 445 nm or 375 nm laser pulse of power P^λ and duration t_p on two representative aged NVs. Promisingly, maximum η^{NV} is sustained for excitation pulses of both wavelengths that deliver less than *ca.* 10 pJ. Thus, for blue and UV pulses of sufficiently short duration or low power, normal ODMR measurements can be performed without the need for re-initialization and the minimum delay t_d^{min} is limited only by the NV⁻ shelving state lifetime of *ca.* 300 ns. Longer delays are required if the perturbing blue or UV pulse exceeding 10 pJ scrambles NV charge and spin state or populates newly formed traps, necessitating re-initialization with a second green laser pulse. **Figure 5d,e** shows the total sensitivity in this regime, expressed as $\eta^{\text{total}} \propto \eta^{\text{NV}} e^{-t_d/\tau_m}$. In the case of 445 nm excitation, the non-zero PLE results in finite η^{total} even for $\tau_d = t_d^{\text{min}}$. In comparison, after the 375 nm pulse, the slow recovery of η^{NV} would preclude sensing of RP species with $\tau_m \leq 10 \mu\text{s}$.

In summary, we characterize the impact of 445 nm and 375 nm laser excitation on the charge and spin dynamics of near-surface NVs. The results agree well with the predicted UV and blue photophysics of NVs expected from a simplified three-level model. Our observations of power-dependent photoionization dynamics under blue illumination and accelerated deterioration of NV sensing properties under UV exposure provide important context to realize the potential of NVs to probe photochemical reactions and radical pair species. We identify a parameter space for both blue and UV laser excitation that would enable sensing of sufficiently long-lived photogenerated radical pairs in proximal molecules. Beyond photochemistry, the results herein provide insight into all-optical charge-state control of spin

defects in diamond. Lastly, permanent aging of NVs proximal to surfaces is a serious challenge for long-term measurements with shallow defects, yet these effects have been described to date mostly anecdotally and remain poorly understood. This work takes an important step toward elucidating degradation of NV electronic environments by tracking the aging process.

Supporting Information

The Supporting Information provides details on materials and experimental methods, including additional data used to evaluate the conclusions in the paper; Figures S1–S5 and Tables S1 and S2 show the instrumentation schematics, charge and spin dynamics under blue and UV illumination for all NVs characterized, saturation curve of a representative NV under 445 nm illumination, and additional experimental details for data presented in the main text figures.

Author Information

Corresponding Authors

Christian L. Degen, *Department of Physics, ETH Zürich, Otto-Stern-Weg 1, 8093 Zürich, Switzerland & Quantum Center, ETH Zürich, 8093 Zürich, Switzerland*, ORCID: 0000-0003-2432-4301, E-mail: degenc@ethz.ch

John M. Abendroth, *Department of Physics, ETH Zürich, Otto-Stern-Weg 1, 8093 Zürich, Switzerland*, ORCID: 0000-0002-2369-4311, E-mail: jabendroth@phys.ethz.ch

Authors

Laura A. Völker, *Department of Physics, ETH Zürich, Otto-Stern-Weg 1, 8093 Zürich, Switzerland*, ORCID: 0000-0002-2990-9301

Konstantin Herb, *Department of Physics, ETH Zürich, Otto-Stern-Weg 1, 8093 Zürich, Switzerland*

Darin A. Merchant, *Department of Physics, ETH Zürich, Otto-Stern-Weg 1, 8093 Zürich, Switzerland*

Lorenzo Bechelli, *Department of Physics, ETH Zürich, Otto-Stern-Weg 1, 8093 Zürich, Switzerland*, ORCID: 0009-0003-4954-2679

Author Contributions

L.A.V., C.L.D., and J.M.A. conceived and designed the experiments. Data were collected by L.A.V., K.H., and D.A.M. All authors discussed the results. The manuscript was written by L.A.V., C.L.D., and J.M.A. with assistance from all other authors.

Notes

The authors declare no competing financial interest.

Acknowledgment

The authors thank Stefan Ernst, Jan Rhensius, Erika Janitz and Tianqi Zhu for insightful discussions. J.M.A. acknowledges funding from the Swiss National Science Foundation (SNSF) Ambizione Project Grant No. PZ00P2-201590. C.L.D. acknowledges funding from the SBFI, Project "QMetMuFuSP" under Grant. No. UeM019-8, 215927 and from the SNSF, under Grants. No. 200021-219386 and CRSII-222812.

References

- (1) Kothe, G.; Weber, S.; Ohmes, E.; Thurnauer, M. C.; Norris, J. R. High Time Resolution Electron Paramagnetic Resonance of Light-Induced Radical Pairs in Photosynthetic Bacterial Reaction Centers: Observation of Quantum Beats. *J. Am. Chem. Soc.* **1994**, *116*, 7729–7734.
- (2) Levanon, H.; Möbius, K. Advanced EPR Spectroscopy on Electron Transfer Processes in Photosynthesis and Biomimetic Model Systems. *Annu. Rev. Biophys.* **1997**, *26*, 495–540.
- (3) Schmermund, L.; Jurkaš, V.; Özgen, F.; Barone, G.; Büchenschütz, H.; Winkler, C.; Schmidt, S.; Kourist, R.; Kroutil, W. Photo-Biocatalysis: Biotransformations in the Presence of Light. *ACS Catal.* **2019**, *9*, 4115–4144.
- (4) Hore, P.; Mouritsen, H. The Radical-Pair Mechanism of Magnetoreception. *Annu. Rev. Biophys.* **2016**, *45*, 299–344.
- (5) Biskup, T.; Schleicher, E.; Okafuji, A.; Link, G.; Hitomi, K.; Getzoff, E.; Weber, S. Direct Observation of a Photoinduced Radical Pair in a Cryptochrome Blue-Light Photoreceptor. *Angew. Chem. Int. Ed.* **2009**, *48*, 404–407.
- (6) Hadi, Z.-H.; Simon, C. Magnetic Field Effects in Biology from the Perspective of the Radical Pair Mechanism. *J. R. Soc. Interface* **2022**, *19*, 20220325.
- (7) Mani, T. Molecular Qubits Based on Photogenerated Spin-Correlated Radical Pairs for Quantum Sensing. *Chem. Phys. Rev.* **2022**, *3*, 021301.
- (8) Rugg, B.; Krzyaniak, M.; Phelan, B.; Ratner, M.; Young, R.; Wasielewski, M. Photo-driven Quantum Teleportation of an Electron Spin State in a Covalent Donor-Acceptor-Radical System. *Nat. Chem.* **2019**, *11*, 981–986.

- (9) Neleson, J.; Zhang, J.; Zhou, J.; Rugg, B.; Krzyaniak, M.; Wasielewski, M. CNOT Gate Operation on a Photogenerated Molecular Electron Spin-Qubit Pair. *J. Chem. Phys.* **2020**, *152*, 014503.
- (10) Mao, H.; Pažera, G. J.; Young, R. M.; Krzyaniak, M. D.; Wasielewski, M. R. Quantum Gate Operations on a Spectrally Addressable Photogenerated Molecular Electron Spin-Qubit Pair. *J. Am. Chem. Soc.* **2023**, *145*, 6585–6593.
- (11) Liu, H.; Plenio, M.; Cai, J. Scheme for Detection of Single-Molecule Radical Pair Reaction Using Spin in Diamond. *Phys. Rev. Lett.* **2017**, *118*, 200402.
- (12) Finkler, A.; Dasari, D. Quantum Sensing and Control of Spin-State Dynamics in the Radical-Pair Mechanism. *Phys. Rev. Appl.* **2021**, *15*, 034066.
- (13) Völker, L. A.; Herb, K.; Janitz, E.; Degen, C. L.; Abendroth, J. M. Toward Quantum Sensing of Chiral Induced Spin Selectivity: Probing Donor-Bridge-Acceptor Molecules with NV Centers in Diamond. *J. Chem. Phys.* **2023**, *158*, 161103.
- (14) Khurana, D.; Jensen, R. H.; Giri, R.; Bocquel, J.; Andersen, U. L.; Berg-Sørensen, K.; Huck, A. Sensing of Magnetic Field Effects in Radical-Pair Reactions using a Quantum Sensor. *Phys. Rev. Res.* **2024**, *6*, 013218.
- (15) Lovchinsky, I.; Sushkov, A. O.; Urbach, E.; de Leon, N. P.; Choi, S.; Greve, K. D.; Evans, R.; Gertner, R.; Bersin, E.; Müller, C.; McGuinness, L.; Jelezko, F.; Walsworth, R. L.; Park, H.; Lukin, M. D. Nuclear Magnetic Resonance Detection and Spectroscopy of Single Proteins using Quantum Logic. *Science* **2016**, *351*, 836–841.
- (16) Janitz, E.; Herb, K.; Völker, L. A.; Huxter, W. S.; Degen, C. L.; Abendroth, J. M. Diamond Surface Engineering for Molecular Sensing with Nitrogen—Vacancy Centers. *J. Mater. Chem. C* **2022**, *10*, 13533–13569.

- (17) Abendroth, J. M.; Herb, K.; Janitz, E.; Zhu, T.; Völker, L. A.; Degen, C. L. Single-Nitrogen-Vacancy NMR of Amine-Functionalized Diamond Surfaces. *Nano Lett.* **2022**, *22*, 7294–7303.
- (18) Liu, K. S.; Ma, X.; Rizzato, R.; Semrau, A. L.; Henning, A.; Sharp, I. D.; Fischer, R. A.; Bucher, D. B. Using Metal-Organic Frameworks to Confine Liquid Samples for Nanoscale NV-NMR. *Nano Lett.* **2022**, *22*, 9876–9882.
- (19) Xie, M.; Yu, X.; Rodgers, L. V. H.; Xu, D.; Chi-Durán, I.; Toros, A.; Quack, N.; de Leon, N. P.; Maurer, P. C. Biocompatible Surface Functionalization Architecture for a Diamond Quantum Sensor. *Proc. Natl. Acad. Sci. U. S. A.* **2022**, *119*, e2114186119.
- (20) Rodgers, L. et al. Diamond Surface Functionalization via Visible Light-Driven C-H Activation for Nanoscale Quantum Sensing. *Proceedings of the National Academy of Sciences* **2024**, *121*, e2316032121.
- (21) Perona Martínez, F.; Nusantara, A. C.; Chipaux, M.; Padamati, S. K.; Schirhagl, R. Nanodiamond Relaxometry-Based Detection of Free-Radical Species When Produced in Chemical Reactions in Biologically Relevant Conditions. *ACS Sensors* **2020**, *5*, 3862–3869.
- (22) Ninio, Y.; Waiskopf, N.; Meirzada, I.; Romach, Y.; Haim, G.; Yochelis, S.; Banin, U.; Bar-Gill, N. High-Sensitivity, High-Resolution Detection of Reactive Oxygen Species Concentration Using NV Centers. *ACS Photonics* **2021**, *8*, 1917–1921.
- (23) Gaebel, T.; Domhan, M.; Wittmann, C.; Popa, I.; Jelezko, F.; Rabeau, J.; Greentree, A.; Prawer, S.; Trajkov, E.; Hemmer, P. R.; Wrachtrup, J. Photochromism in Single Nitrogen-Vacancy Defect in Diamond. *Applied Physics B* **2006**, *82*, 243–246.
- (24) Waldherr, G.; Beck, J.; Steiner, M.; Neumann, P.; Gali, A.; Frauenheim, T.; Jelezko, F.; Wrachtrup, J. Dark States of Single Nitrogen-Vacancy Centers in Diamond Unraveled by Single Shot NMR. *Phys. Rev. Lett.* **2011**, *106*, 157601.

- (25) Beha, K.; Batalov, A.; Manson, N. B.; Bratschitsch, R.; Leitenstorfer, A. Optimum Photoluminescence Excitation and Recharging Cycle of Single Nitrogen-Vacancy Centers in Ultrapure Diamond. *Phys. Rev. Lett.* **2012**, *109*, 097404.
- (26) Aslam, N.; Waldherr, G.; Neumann, P.; Jelezko, F.; Wrachtrup, J. Photo-Induced Ionization Dynamics of the Nitrogen Vacancy Defect in Diamond Investigated by Single-Shot Charge State Detection. *New J. Phys.* **2013**, *15*, 013604.
- (27) Hacquebard, L.; Childress, L. Charge-State Dynamics During Excitation and Depletion of the Nitrogen-Vacancy Center in Diamond. *Phys. Rev. A* **2018**, *97*, 063408.
- (28) Razinkovas, L.; Maciaszek, M.; Reinhard, F.; Doherty, M. W.; Alkauskas, A. Photoionization of Negatively Charged NV Centers in Diamond: Theory and ab initio Calculations. *Phys. Rev. B* **2021**, *104*, 235301.
- (29) Han, K. Y.; Kim, S. K.; Eggeling, C.; Hell, S. W. Metastable Dark States Enable Ground State Depletion Microscopy of Nitrogen Vacancy Centers in Diamond with Diffraction-Unlimited Resolution. *Nano Lett.* **2010**, *10*, 3199–3203.
- (30) Chen, C.-D.; Zou, C.-L.; Sun, F.-W.; Guo, G.-C. Optical Manipulation of the Charge State of Nitrogen-Vacancy Center in Diamond. *Appl. Phys. Lett.* **2013**, *103*, 013112.
- (31) Bourgeois, E.; Londero, E.; Buczak, K.; Hruby, J.; Gulka, M.; Balasubramaniam, Y.; Wachter, G.; Stursa, J.; Dobes, K.; Aumayr, F.; Trupke, M.; Gali, A.; Nesladek, M. Enhanced Photoelectric Detection of NV Magnetic Resonances in Diamond Under Dual-Beam Excitation. *Phys. Rev. B* **2017**, *95*, 041402.
- (32) Li, C.; Zhang, Q.; Zhou, N.; Hu, B.; Ma, C.; Zhang, C.; Yi, Z. UV-Induced Charge-State Conversion from the Negatively to Neutrally Charged Nitrogen-Vacancy Centers in Diamond. *J. Appl. Phys.* **2022**, *132*, 215102.

- (33) Yang, T.; Huang, Y.-W.; Bista, P.; Ding, C.-F.; Chen, J.; Chiang, H.-C., C.-T. Chang Photoluminescence of Nitrogen-Vacancy Centers by Ultraviolet One- and Two-Photon Excitation of Fluorescent Nanodiamonds. *J. Phys. Chem. Lett.* **2022**, *13*, 11280–11287.
- (34) Wood, A. A.; Lozovoi, A.; Goldblatt, R. M.; Meriles, C. A.; Martin, A. M. Wavelength Dependence of Nitrogen Vacancy Center Charge Cycling. *Phys. Rev. B* **2024**, *109*, 134106.
- (35) Bradac, C.; Gaebel, T.; Naidoo, N.; Sellars, M. J.; Twamley, J.; Brown, L. J.; Barnard, A. S.; Plakhotnik, T.; Zvyagin, A. V.; Rabeau, J. R. Observation and Control of Blinking Nitrogen-Vacancy Centres in Discrete Nanodiamonds. *Nature Nanotechnology* **2010**, *5*, 345–349.
- (36) Dhomkar, S.; Jayakumar, H.; Zangara, P.; Meriles, C. Charge Dynamics in Near-Surface, Variable-Density Ensembles of Nitrogen-Vacancy Centers in Diamond. *Nano Lett.* **2018**, *18*, 4046–4052.
- (37) Sangtawesin, S. et al. Origins of Diamond Surface Noise Probed by Correlating Single-Spin Measurements with Surface Spectroscopy. *Phys. Rev. X* **2019**, *9*, 031052.
- (38) Bluvstein, D.; Zhang, Z.; Jayich, A. C. B. Identifying and Mitigating Charge Instabilities in Shallow Diamond Nitrogen-Vacancy Centers. *Phys. Rev. Lett.* **2019**, *122*, 076101.
- (39) Yuan, Z.; Fitzpatrick, M.; Rodgers, L. V. H.; Sangtawesin, S.; Srinivasan, S.; de Leon, N. P. Charge State Dynamics and Optically Detected Electron Spin Resonance Contrast of Shallow Nitrogen-Vacancy Centers in Diamond. *Phys. Rev. Res.* **2020**, *2*, 033263.
- (40) Shields, B. J.; Unterreithmeier, Q. P.; de Leon, N. P.; Park, H.; Lukin, M. D. Efficient Readout of a Single Spin State in Diamond via Spin-to-Charge Conversion. *Phys. Rev. Lett.* **2015**, *114*, 136402.

- (41) Hopper, D.; Grote, R.; Parks, S.; Bassett, L. Amplified Sensitivity of Nitrogen-Vacancy Spins in Nanodiamonds Using All-Optical Charge Readout. *ACS Nano* **2018**, *12*, 4678–4686.
- (42) Ernst, S.; Scheidegger, P. J.; Diesch, S.; Lorenzelli, L.; Degen, C. L. Temperature Dependence of Photoluminescence Intensity and Spin Contrast in Nitrogen-Vacancy Centers. *Phys. Rev. Lett.* **2023**, *131*, 086903.
- (43) Deák, P.; Aradi, B.; Kaviani, M.; Frauenheim, T.; Gali, A. Formation of NV Centers in Diamond: A Theoretical Study Based on Calculated Transitions and Migration of Nitrogen and Vacancy Related Defects. *Phys. Rev. B* **2014**, *89*, 075203.
- (44) Zhu, T.; Rhensius, J.; Herb, K.; Damle, V.; Puebla-Hellmann, G.; Degen, C. L.; Janitz, E. Multicone Diamond Waveguides for Nanoscale Quantum Sensing. *Nano Lett.* **2023**, *23*, 10110–10117.
- (45) Manson, N.; Harrison, J. Photo-Ionization of the Nitrogen-Vacancy Center in Diamond. *Diam. Relat. Mater.* **2005**, *14*, 1705–1710.
- (46) Luo, T.; Lindner, L.; Langer, J.; Cimalla, V.; Vidal, X.; Hahl, F.; Schreyvogel, C.; Onoda, S.; Ishii, S.; Ohshima, T. Creation of Nitrogen-Vacancy Centers in Chemical Vapor Deposition Diamond for Sensing Applications. *New J. Phys.* **2022**, *24*, 033030.
- (47) Miyamoto, Y. Decay Process of Photoexcited Divacancies in Diamond Studied by First-Principles Simulations. *Phys. Rev. Mater.* **2023**, *7*, 086002.
- (48) Neethirajan, J.; Hache, T.; Paone, D.; Pinto, D.; Denisenko, A.; Stöhr, R.; Udvarhelyi, P.; Pershin, A.; Gali, A.; Wrachtrup, J.; Kern, K.; Singha, A. Controlled Surface Modification to Revive Shallow NV⁻ Centers. *Nano Lett.* **2023**, *23*, 2563–2569.

Supplementary Information:
Charge and Spin Dynamics and Destabilization of
Shallow Nitrogen–Vacancy Centers under UV
and Blue Excitation

Laura A. Völker¹, Konstantin Herb¹, Darin A. Merchant¹, Lorenzo Bechelli¹,
Christian L. Degen^{1,2,*} and John M. Abendroth^{1*}

¹*Department of Physics, ETH Zürich, Otto-Stern-Weg 1, 8093 Zürich, Switzerland*

²*Quantum Center, ETH Zürich, 8093 Zürich, Switzerland*

E-mail: degenc@phys.ethz.ch; jabendroth@phys.ethz.ch

Materials and Methods

Diamond Sample Preparation

A commercially available diamond membrane with nanofabricated pillar arrays containing shallow NV centers was used in this study (QZabre Ltd, Zürich, CH). The membrane is a quantum-grade (001)-terminated single-crystalline CVD-grown diamond (Element Six, Didcot, UK). The membrane was implanted with $^{15}\text{N}^+$ ions at 7 keV energy (CuttingEdge Ions, LLC; Anaheim, CA, USA) yielding an expected mean implantation depth of 10.8(40) nm determined using The Stopping and Range of Ions in Matter (SRIM) simulations.^{S1} The membrane was annealed at 880 °C for 2 h to convert implanted nitrogen into NV centers due to vacancy migration. Following annealing, nanopillar waveguide arrays hosting nominally single NV centers were fabricated by electron-beam lithography and reactive-ion etching.^{S2} The as-received membrane was cleaned for *ca.* 2 h in a 1:1:1 tri-acid mixture of $\text{H}_2\text{SO}_4:\text{HClO}_4:\text{HNO}_3$ at 120 °C, baked at 460 °C under oxygen atmosphere (AS-Micro, RTP-System, Annealsys; Montpellier, FR) for 4 h, and then cleaned in piranha solution (3:1 $\text{H}_2\text{SO}_4:\text{H}_2\text{O}_2$) before measuring.

Confocal Microscope for NV Measurements and Microwave Instrumentation

Experiments were performed on a custom-built confocal microscope, equipped with four different lasers at 375 nm (Toptica iBeam Smart 375 diode laser), 445 nm (homebuilt laser using diodes purchased from Frankfurt Laser), 520 nm (homebuilt laser using diode purchased from Frankfurt Laser) and 594 nm (Cobolt Mambo 594 diode-pumped solid-state laser) and a 625–800 nm detection path. A schematic depiction of the setup is provided in Figure **S1**. Optical pulses were generated either by using an acousto optic modulator (594 nm) or by direct modulation of diode drive current (375 nm, 445 nm, 520 nm). Lasers were focused on the sample with a high NA objective (Olympuys UPLXAPO 40×). Photons emitted from

the diamond sample were detected with a single-photon avalanche photodiode (Excelitas SPCM-AQRH family), time-tagged (NI-PCIe-6363) and software-binned.

Microwave pulses were synthesized using an arbitrary-waveform generator (Spectrum Instrumentation DN2.663-04) and up-converted by a vector signal generator (Stanford Research Systems SG-386). They were amplified (Mini Circuits High Power Amplifier ZHL-15W-422-S+) and delivered to the sample through a home-built coplanar waveguide. A static bias field B_0 was generated using a cylindrical samarium cobalt permanent magnet (TC-SmCo). Alignment of B_0 with the NV centers ZFS crystal axis was achieved by physically moving the magnet.

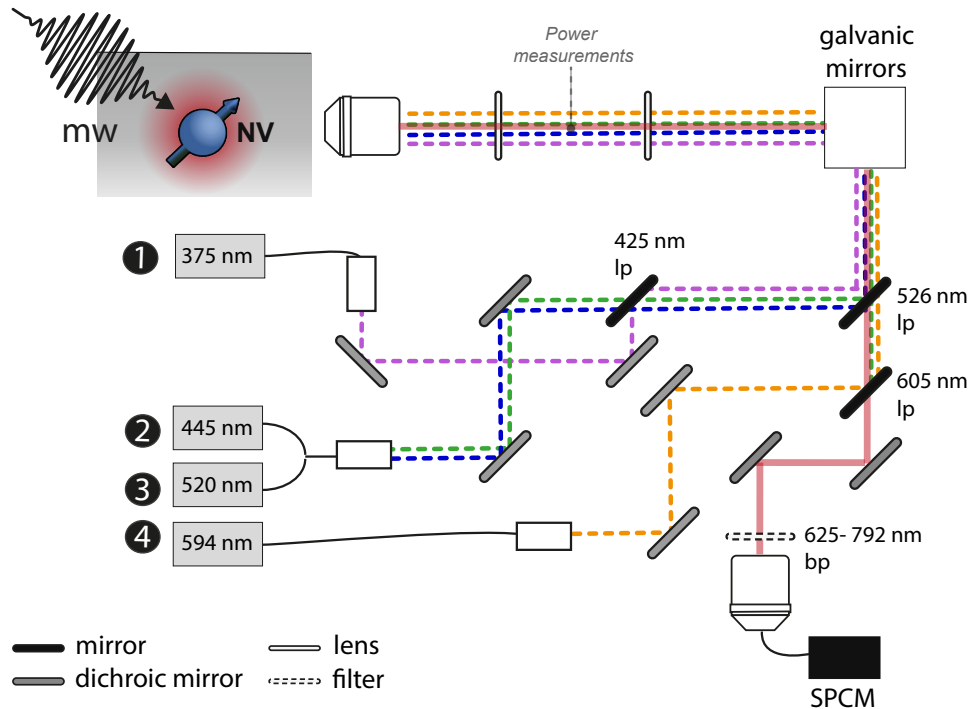


Figure S1: Schematic layout of home-built confocal microscope utilized in this study. For dichroic mirrors and filters, relevant wavelengths are specified (lp = longpass, bp = band-pass).

Estimation of Laser Powers

Laser powers reported in the main text refer to power at the sample. These values were estimated by measuring the power (Thorlabs C-series power sensor with S120VC sensor

head) at the latest accessible point in the optical path (middle of 4f-system, see Figure S1) and correcting for losses through the remaining components using the transmission data provided by the respective manufacturers.

NV Center Characterization

NV centers were selected in nanopillar waveguide arrays hosting nominally single emitters based on sufficiently high fluorescence intensity under green laser illumination. Resonance frequencies were determined by continuous-wave optically detected magnetic resonance (cw-ODMR) experiments and microwave pulse lengths were calibrated *via* Rabi-measurements. All measurements of this study were performed at a magnetic bias field of ≈ 10 mT (*i.e.*, resonance frequencies of ≈ 2.59 GHz) and at Rabi-frequencies of ≈ 7 MHz. Laser pulses were followed by $2\ \mu\text{s}$ delays. Charge and spin state init was performed using 0.08 mW green laser illumination. Readout was performed using 0.3 mW orange illumination and fluorescence counts were integrated for 300 ns. Ionization dynamics were characterized by pulsed ODMR measurements at the NV centers resonance frequency for a series of ionizing pulses of varying length t_p (see main text Figure 1(d) for pulse sequences). Reference measurements without the ionizing pulse were taken simultaneously. Other relevant parameters are provided in Table S1.

Table S1: Experimental details (pulse length, laser powers, *etc.*) for measurement data shown in main text figures.

Fig.	Panel	Details
2	a, b	Blue ionization as a function of blue laser pulse length: NV was initialized with a $15\ \mu\text{s}$ green laser pulse. Ionization under 445 nm illumination was probed for pulse lengths ranging from 100 ns – 4 ms and laser powers ranging from 0.1 mW to >1 mW.

	c, d	UV ionization as a function of UV laser pulse length: NV was initialized with a 250 μs green laser pulse. Ionization under 375 nm illumination was probed for pulse lengths ranging from 100 ns – 2 ms and laser powers ranging from 0.01 mW to >0.1 mW.
3	a, b bottom, c bottom	Ionization rates under orange laser illumination: NV centers were initialized with 15 μs green laser pulses and ionized using orange laser pulses of varying lengths, ranging from 100 ns to several ms. Ionization rates were extracted via least squares fitting.
	b top	Steady state NV^- fraction remaining under blue laser illumination. NVs were initialized with a 15 μs green laser pulse. Ionization was induced using a 0.016 mW 445 nm laser pulse of sufficient length (determined in ionization measurement, typically ≥ 250 μs).
	c top	Steady state NV^- fraction remaining under UV laser illumination. NVs were initialized with a > 250 μs green laser pulse (longer pulses required for aged NV centers due to altered recombination). Ionization was induced using a 375 nm (powers ranging from 0.024 mW to 0.069 mW) laser pulse of sufficient length (determined in ionization measurement, typically ≥ 250 μs).
4	a	Recombination after blue induced illumination on NV centers that had been aged using blue laser light. NVs were fully ionized using 500 μs , 0.016 mW 445 nm laser pulses (Ionizing pulse length and power were chosen based on ionization measurement). Recombination was performed using green laser pulses with pulse lengths ranging from 100 ns – 2 ms.

	b	Recombination after UV induced illumination on NV centers that had been aged using UV laser light. NV centers were fully ionized using 250 μ s, 0.024 mW to 0.069 mW 375 nm illumination. (Ionizing pulse length and power were chosen based on ionization measurement). Recombination was performed using green laser pulses with pulse length ranging from 100 ns – 2 ms.
	c	Recombination after i) orange, ii) blue and iii) UV induced illumination, measured on the same NV center after UV induced aging. The NV center was ionized using sufficiently long (>250 μ s) pulses of the respective color. In each case pulse length was chosen based on an ionization measurement. For 445 nm, ionization was performed at 0.010 mW, for UV illumination at 0.034 mW. The recombination was performed using green laser pulses with pulse lengths ranging from 100 ns – 2 ms.
5	b	NV sensitivity evolution as a function of blue exposure dose. Sensitivity was evaluated based on an ionization measurement performed under the following conditions. The NV was initialized with a 15 μ s green laser pulse. Ionization under 445 nm illumination was probed for pulse lengths ranging from 100 ns – 4 ms at a laser powers of 0.016 mW.
	c	NV sensitivity evolution as a function of UV exposure dose. Sensitivity was evaluated based on an ionization measurement performed under the following conditions. The NV was initialized with a 1000 μ s green laser pulse. Ionization under 375 nm illumination was probed for pulse lengths ranging from 100 ns – 4 ms at a laser power of 0.034 mW.

d

NV sensitivity evolution as a function of green recombination pulse length. The sensitivity was evaluated based on a recombination measurement performed under the following conditions. The NV was fully ionized with a 500 μs , 0.016 mW blue laser pulse. The recombination was performed using green laser pulses with pulse lengths ranging from 100 ns – 2 ms.

e

NV sensitivity evolution as a function of green recombination pulse length. The sensitivity was evaluated based on a recombination measurement performed under the following conditions. The NV was fully ionized with a 250 μs , 0.034 mW UV laser pulse. The recombination was performed using green laser pulses with pulse lengths ranging from 100 ns – 2 ms.

Three Level Rate Model

To physically motivate the mathematical form of the acquired ionization/recombination traces, we utilize a simplified three level model, consisting of two levels (M_0 and M_1) for spin states $m_S = 0$ and $m_S = \pm 1$, respectively for NV^- and a single level (Z) for NV^0 . Charge and spin dynamics are parameterized using spin-dependent ionization rates $k_{i,0}$ and $k_{i,1}$ from the $m_S = 0$ and $m_S = \pm 1$ spin states, spin state polarization with a rate k_s and recombination at a rate k_r . Since ionization events do not necessarily preserve the spin state, we assume that reionization equally populates all spin levels of NV^- . The evolution of level populations is a system of three coupled differential equations,

$$\frac{d\vec{N}}{dt} = \begin{pmatrix} -k_{i,0} & k_s & k_r \\ 0 & -k_{i,1} - k_s & 2k_r \\ k_{i,0} & k_{i,1} & -3k_r \end{pmatrix} \cdot \begin{pmatrix} M_0 \\ M_1 \\ Z \end{pmatrix}. \quad (1)$$

Starting from a negatively charged NV center with fully polarized spin state, *i.e.*, $\vec{N}(0) = (1, 0, 0)$ the population of NV^0 evolves in a bi-exponential manner,

$$Z(t_p) = \alpha e^{-t/\tau_1} + \beta e^{-t/\tau_2} + \gamma \quad (2)$$

with

$$\tau_1 = \frac{1}{(k_{i,0} + k_s + k_{i,1} + 3k_r) + k_w} \quad (3)$$

$$\tau_2 = \frac{1}{(k_{i,0} + k_s + k_{i,1} + 3k_r) - k_w} \quad (4)$$

where we have introduced

$$k_w = \sqrt{(-k_{i,0} + k_s + k_{i,1})^2 - 2(k_{i,0} + 3k_s - k_{i,1})k_r + 9k_r^2}. \quad (5)$$

However, if one assumes that $k_{i,0} = k_{i,1} = k_i$ this simplifies to

$$Z(t_p) = \alpha e^{-t/\tau_1} + \gamma \quad (6)$$

with

$$\tau_1 = \frac{1}{(k_i + 3k_r)}. \quad (7)$$

For recombination processes, an analogue evaluation can be performed, starting from $\vec{N}(0) = (0, 0, 1)$.

Data Analysis

Calculation of ρ and c

Under orange laser excitation, only populations M_0 and M_1 contribute to the fluorescence signal since excitation occurs in a charge-state selective manner. Thus, our experimental observables, the time averaged photoluminescence intensities in the signal and reference traces of the ODMR

experiment (I_{sig} and I_{ref}) are directly proportional to M_0 and M_1 . For I_{ref} , we define

$$I_{\text{ref}} = \epsilon_0 M_0 + \epsilon_1 M_1 + \epsilon_{-1} M_{-1} = \epsilon_0 M_0 + 2\epsilon_1 M_1 \quad (8)$$

where we have introduced ϵ_i ($i = 0, \pm 1$) as proportionality factors transferring level populations for a spin state $m_S = i$ to fluorescence counts. For the NV center $\epsilon_0 \gg \epsilon_1$. Also, $M_1 = M_{-1}$ and $\epsilon_1 = \epsilon_{-1}$. The π -pulse of the ODMR experiment swaps the populations of the $m_S = 0$ and $m_S = 1$ levels, resulting in

$$I_{\text{sig}} = \epsilon_0 M_1 + \epsilon_1 M_0 + \epsilon_1 M_1 = (\epsilon_0 + \epsilon_1) M_1 + \epsilon_1 M_0. \quad (9)$$

As a proxy for spin state polarization, we define ODMR contrast c

$$c = \frac{I_{\text{ref}} - I_{\text{sig}}}{I_{\text{ref}}} = \frac{(\epsilon_0 - \epsilon_1)(M_0 - M_1)}{\epsilon_0 M_0 + 2\epsilon_1 M_1} \approx \frac{\epsilon_0(M_0 - M_1)}{\epsilon_0 M_0} = \frac{M_0 - M_1}{M_0} \quad (10)$$

where we have set ϵ_1 to zero, since $\epsilon_0 \gg \epsilon_1$. To estimate the relative population ρ of the NV^- charge state from the experimental data, we use the linear combination

$$\frac{1}{3} I_{\text{ref}} + \frac{2}{3} I_{\text{sig}} \propto M_0 + M_1 + M_{-1} \propto \rho \quad (11)$$

which is independent of c and reference it to the contrast - corrected value of the ODMR signal after green charge state initialization.

Fitting

The time evolutions of the signal and reference traces of an ODMR experiment as a function of ionizing/recombining laser pulse length, $c_{\text{ODMR}}^{\text{ref}}(t)$ and $c_{\text{ODMR}}^{\text{sig}}(t)$, were fit simultaneously to

$$c_{\text{ODMR}}^{\text{ref}}(t) = \gamma_1 + \alpha_1 \exp -t/\tau_1 \quad (12)$$

$$c_{\text{ODMR}}^{\text{sig}}(t) = \gamma_1 + \gamma_2 + \alpha_2 \exp -t/\tau_1 \quad (13)$$

for the mono-exponential case and

$$c_{\text{ODMR}}^{\text{ref}}(t) = \gamma_1 + \alpha_1 \exp -t/\tau_1 + \beta_1 \exp -t/\tau_2 \quad (14)$$

$$c_{\text{ODMR}}^{\text{sig}}(t) = \gamma_1 + \gamma_2 + \alpha_2 \exp -t/\tau_1 + \beta_2 \exp -t/\tau_2 \quad (15)$$

for the bi-exponential case. Fit uncertainties were extracted with a bootstrapping approach.

Additional Results and Data

Table S2: Numerical results for ODMR contrast and orange ionization rates, before (b) and after (a) UV/blue induced aging with total energy E . Numerical values are reported with 95% confidence intervals.

NV	c^{520} (b) [%]	c^{520} (a) [%]	k_i^{594} (b) [MHz]	k_i^{594} (a) [MHz]	E [mJ]
1	41.6(6)	-	0.160(7)	-	-
2	39.2(7)	-	0.132(8)	-	-
3	26(3)	-	0.15(2)	-	-
4	9.8(7)	-	0.25(3)	-	-
5	36.6(7)	-	0.8(1)	-	-
6	38.6(6)	-	0.28(2)	-	-
7	35.1(8)	-	0.19(2)	-	-
8	38.7(4)	-	0.22(1)	-	-
Blue Set					
◁	39.4(5)	38.7(6)	0.30(1)	0.27(1)	6625
+	41.0(5)	38.7(6)	0.038(1)	0.174(5)	5583
◇	35.7(8)	37(1)	0.012(2)	0.035(3)	3577
UV Set					
▷	38.1(4)	34(1)	0.55(5)	1.1(2)	201
★	40.6(1)	27(3)	0.161(8)	0.7(1)	373
×	41.9(8)	32(2)	0.026(1)	0.10(2)	938
◇	38(2)	36(2)	0.005(1)	0.026(5)	136

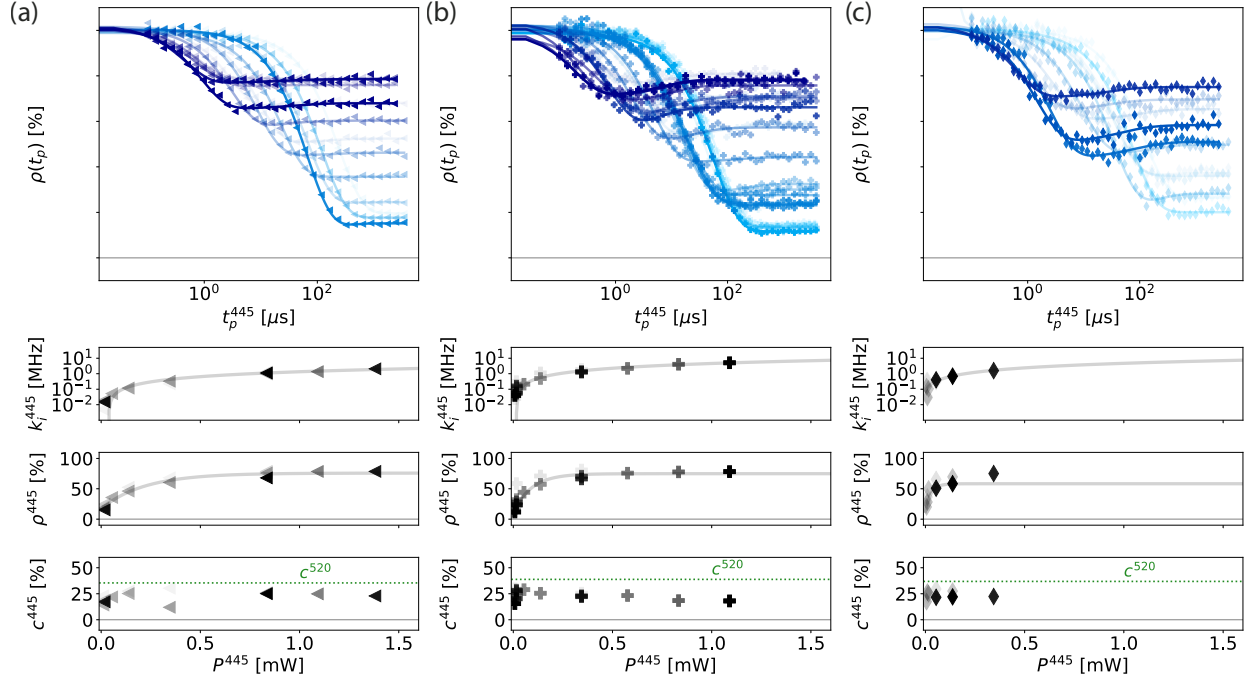


Figure S2: Additional data for charge and spin dynamics of NV center under 445 nm illumination. For three representative NV centers the following data are shown. *Top:* Evolution of NV^- fraction as a function of blue pulse lengths. The color of the curve indicates the blue laser power, ranging from ~ 0.1 mW to 1 mW. The opacity of the curves encode the amount of blue laser light the NV center had already been exposed to when the measurement was taken. Very transparent curves were taken first, on pristine NV centers, while opaque curves show data for 445-aged NV centers. *Bottom:* Ionization rates k_i^{445} , steady state ρ^{445} and c^{445} as a function of P^{445} ; extracted from the curves shown in the top plot. Again, opacity encodes the age of the NV center. For k_i^{445} a linear fit, for steady state ρ^{445} an exponential fit were performed and are in good agreement with the data. For c^{445} the contrast of the NV center under green illumination, c^{520} , is indicated with a green dashed line as a reference.

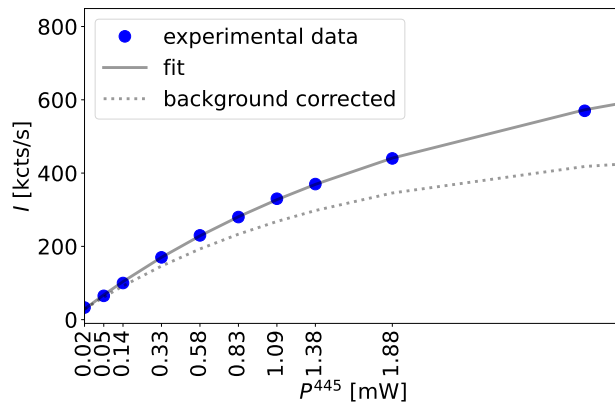


Figure S3: Saturation curve of a representative NV center under 445 nm illumination. Since saturation of NV^- under 445 nm excitation occurs at powers exceeding 1 mW, ODMR contrast c is independent of P^{445} in our measurements performed at blue powers ≤ 1 mW.

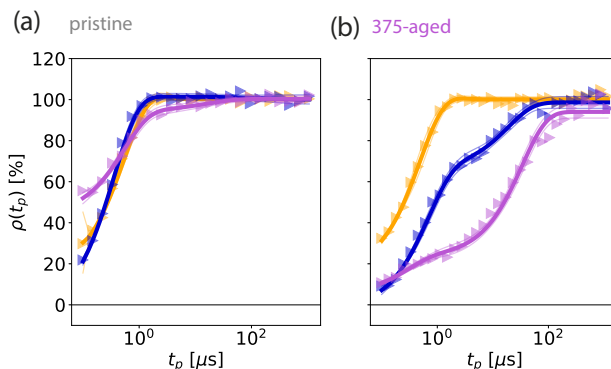


Figure S4: Recombination after i) orange, ii) blue and iii) UV induced illumination, measured on the same NV center before (a) and after (b) UV induced aging. The NV center was ionized using sufficiently long (> 250 μ s) pulses of the respective color. In each case pulse lengths was chosen based on an ionization measurement. For 594 nm and 445 nm, ionization was performed at the same laser powers for both measurements (0.010 mW for blue). For UV illumination laser powers were 0.069 mW and 0.034 mW for measurements on the fresh and the aged NV center, respectively. The recombination was performed using green laser pulses with pulse lengths ranging from 100 ns – 2 ms.

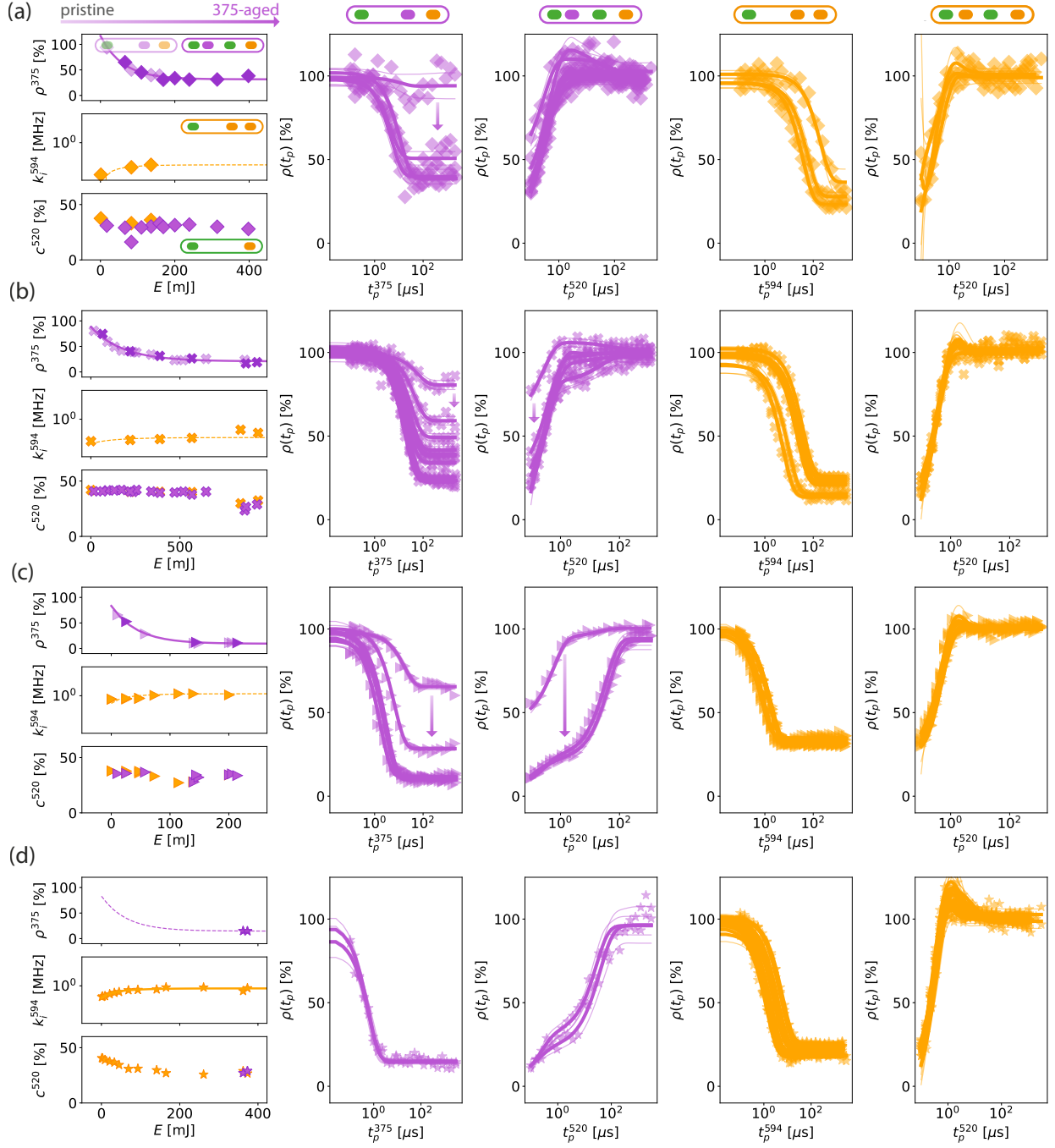


Figure S5: Additional data for aging of NV charge environment induced by UV illumination. Each panel a-d shows data for a separate NV center. *Left:* Evolution of ρ^{375} , k_i^{594} and c^{520} as a function of exposure dose. For ρ^{375} , opaque data points indicate that at this point a recombination measurement was performed; for transparent data points ρ^{375} was determined from the first data point of a recombination measurement. *From second-left to right:* Ionization under UV/orange laser illumination and recombination after UV/orange induced ionization.

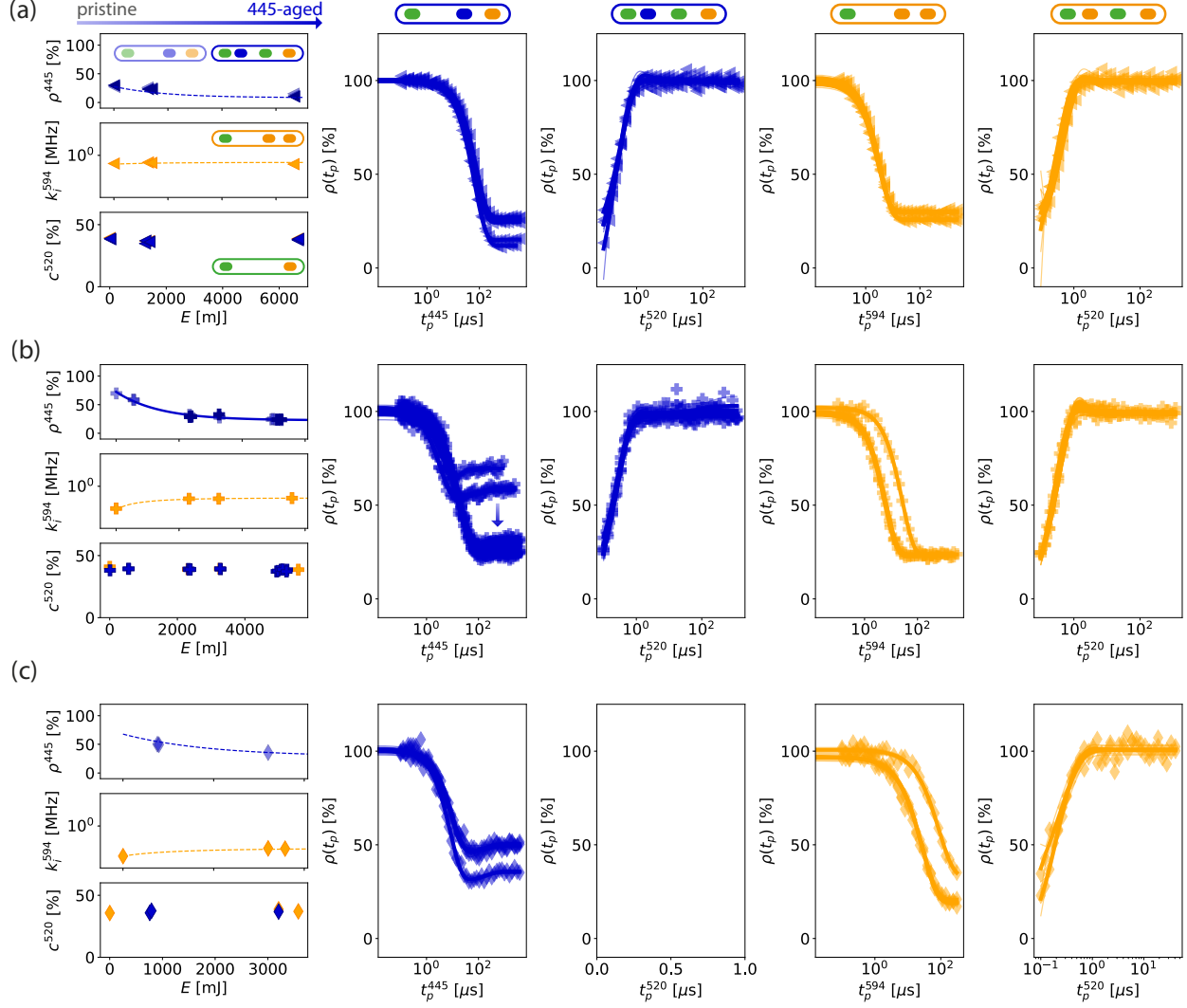


Figure S6: Additional data for aging of NV charge environment induced by blue light illumination. Each panel a-c shows data for a separate NV center. *Left:* Evolution of ρ^{445} , k_i^{594} and c^{520} as a function of exposure dose. For ρ^{445} , opaque data points indicate that at this point a recombination measurement was performed; for transparent data points ρ^{445} was determined from the first data point of a recombination measurement. *From second-left to right:* Ionization under blue/orange laser illumination and recombination after blue/orange induced ionization.

References

- [S1] Ziegler, J.; Ziegler, M.; Biersack, J. SRIM – The Stopping and Range of Ions in Matter (2010).
Nucl. Instrum. Methods Phys. Res. B: Beam Interact. Mater. At. **2010**, *268*, 1818–1823.
- [S2] Zhu, T.; Rhensius, J.; Herb, K.; Damle, V.; Puebla-Hellmann, G.; Degen, C. L.; Janitz, E.
Multicone Diamond Waveguides for Nanoscale Quantum Sensing. *Nano Lett.* **2023**, *23*, 10110–
10117.